JOURNAL OF MATERIALS SCIENCE 32 (1997) 6075–6084

Alumina-coated hollow glass spheres/alumina composites

S. J. WU, L. C. DE JONGHE
Lawrence Berkeley National Laboratory, Materials Science Division, and Department of Materials Science and Mineral Engineering, University of California, Berkeley, CA 94720 USA

Coating of alumina onto the surface of hollow glass spheres was accomplished by controlled heterogeneous precipitation from aqueous solutions. The processing conditions were optimized to yield thin and uniform precursor coatings. After calcination, converting the precursor to alumina, the alumina-coated hollow glass spheres formed free-flowing powders that were used to produce glass/alumina composites with up to 35 vol % of controlled and well dispersed closed porosity. The dielectric constants and the flexural strengths of such porous composites were determined as a function of porosity.

1. Introduction

A variety of techniques have been employed to deposit coatings from solutions onto suspended core particles. Generally, these involve either a physical heterocoagulation or a direct chemical precipitation. In colloidal heterocoagulation [1–3], electrostatically stabilized suspensions of large core particles and small coating particles are brought together. This technique is necessarily limited to systems where the two types of particles can maintain opposite surface charges at the same pH. Also, the surface deposition tends to be limited essentially to a monoparticle layer [2], restricting further the scope of this method.

Several heterogeneous precipitation techniques have been investigated to produce thin coating layers of ceramics or ceramic precursors on core particles [4–11]. Kapolnek [4] first developed a controlled aqueous heterogeneous precipitation method by which a thin layer of an alumina precursor was deposited onto the surface of SiC whiskers. The coating was then thermally converted into alumina. In the present study, the same technique was used to form a thin layer of alumina onto the surface of glass hollow spheres. With these, sintered composites were produced consisting of a dispersion of the coated spheres in an alumina matrix. The experiments demonstrated the possibility of manipulating the microstructure of porous composites to achieve high fractions of isolated pores, while retaining hermeticity and acceptable strength. Such materials may be useful for their dielectric properties, and dielectric constants were therefore also determined as a function of porosity. Relative dielectric constants as low as 5 were obtained for the porous composites.

2. Experimental procedure

2.1. Coating procedures

Commercial hollow glass spheres in the micrometre size range were used (Eccospheres SDT60. Grace Syntactics, Inc.). Table 1 lists some of their important properties. These spheres are basically a borosilicate glass with low alkali content. They were chosen as the porosity-adding material because of their small size, spherical shape, low density, and good handling strength. Scanning electron microscopy (SEM), Fig. 1, showed the as-received spheres to be intact, with only a small fraction of broken spheres and a few large spheres (40–60 μm). The debris and the large particles were removed by passing the spheres through a 37 μm mesh sieve before they were added to distilled water. Because the density of intact hollow spheres ($0.51\ g\,cm^{-3}$) was lower than that of water, they floated on top, while the debris as well as solid particles settled to the bottom. The floating portion was then carefully removed and dried. About 90 wt % of the starting material was retained. SEM examination of the classified powders showed only intact spheres ranging from 5–37 μm, with an average diameter of 21 μm and a standard deviation of 10 μm. The size distribution of the spheres was determined from SEM micrographs by measuring 500 individual particles, and showed a good fit to a normal Gaussian distribution.

Glass wall thickness was determined by crushing some spheres and examining the broken pieces in the SEM. The wall thicknesses ranged between 0.8–1.2 μm. However, a small amount of spheres with very thin walls ($\leqslant 0.5$ μm) were also found. Since they were made of glass the walls were fully dense, the average void fraction of the glass spheres could be calculated to be about 0.74.

Fig. 2 shows the flow chart of the coating procedures. The experiments were carried out in a flat-bottomed flask immersed in a controlled temperature oil bath. Analytic reagent-grade chemicals and distilled water were used. 0.01 M aluminium sulfate hydrate, $Al_2(SO_4)_3 \cdot 18H_2O$ (Fisher Scientific Co.), and 0.02 M urea, $Co(NH_2)_2$ (J. T. Baker, Co.) were first dissolved completely in distilled water. Urea provided a stable

0022–2461

TABLE 1 Typical properties of the hollow glass spheres

Physical:		
	Density ($g\,cc^{-1}$)	0.5
	Softening point (°C)	900
	Wall thickness (μm)[a]	0.8–1.2
	Average diameter (μm)[a]	21
	Standard deviation (μm)[a]	10
	Strength – % Collapse	
	500	1
	1000	2
	2000	4
	4000	7
Chemical: (wt %)		
	SiO_2	93
	B_2O_3	3
	Na_2O	2
	BaO	1
Electrical:		
Dielectric constant (1–8.6 GHz)		1.430
Dissipation factor (1–8.6 GHz)		0.003

[a] data obtained in this study

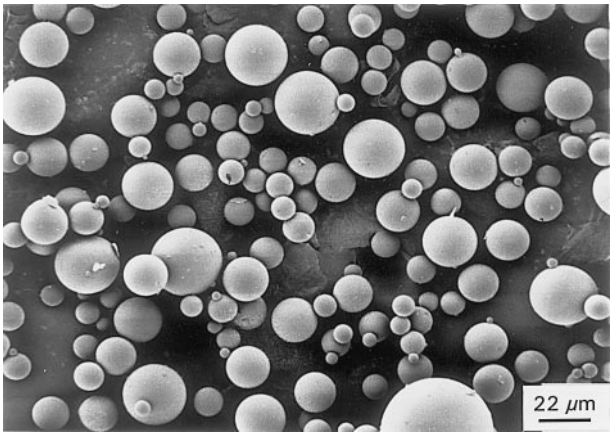

Figure 1 SEM micrograph of as-received hollow glass spheres illustrating the good spherical shapes and the wide size distribution.

supply of the hydroxyl necessary for the precipitation reaction [12]. The solution was passed through a 0.22 μm filter to remove any undissolved materials, and the classified hollow glass spheres were added. Because the composition of the deposited alumina precursor could not be determined precisely the optimal concentration of hollow spheres needed to be found by trial-and-error until an acceptable coating layer was obtained.

The suspension was slowly heated to 95 ± 1 °C, and was held at this temperature, under reflux, for 12 h. Vigorous stirring of the solution was needed to maintain the dispersion of the hollow spheres and reactants.

Upon completion of the heating period, the flask was removed from the oil bath and allowed to stand. After coating the spheres had a higher density than water, and therefore would settle. The supernatant was separated and discarded. Any uncoated spheres would float on the surface of the solution and were removed together with the supernatant. The remaining coated spheres were collected on a filter, rinsed repeatedly with distilled water, and air dried. The dried spheres were heated at constant rate of 1 °C per min., in static air, in an alumina crucible, and calcined at 1150 °C, for 2 h, converting the alumina precursor into α-alumina. Coated spheres before and after calcination were characterized by SEM and X-ray diffraction (XRD). Powder XRD patterns were obtained with a diffractometer (model D500, Siemens A. G., Germany) using Cu K_α radiation over a range of $2\theta = 5$–65 deg. The chemical composition of the coating layer after calcination was determined by energy dispersive X-ray spectroscopy (EDS) in the SEM. Wet chemical analysis (Metallurgical Laboratories, Inc. San Francisco, CA) verified the results obtained from the EDS analysis. Rutherford backscattering spectrometry (RBS) analysed for trace amounts of sulfur which might remain after calcination. The true density of coated spheres after calcination was measured with a helium gas pycnometer (Corning Laboratory Services).

2.2. Composite processing and evaluation

Composite samples with AKP53 α-alumina (Sumitomo Chemical America, Inc.) as the matrix phase and coated spheres as the dispersed second phase were prepared according to the flow chart shown in Fig. 2. Careful control of slip casting was required to avoid any segregation during consolidation of the slurry. Densification studies were performed on a high temperature (Orton Co., Westerville, OH) dilatometer at a constant heating rate of 5 °C per min to 1400 °C, in air. SEM, EDS, and XRD were used to characterize the sintered samples. For SEM examination, sintered samples were cross-sectioned parallel to the slip casting direction to examine for possible segregation during the green body formation. The volume fraction of porosity was determined from linear intercepts on five randomly chosen areas of each of the polished surfaces.

Mechanical strengths were evaluated in a four-point flexure mode with an inner span of 6 mm. Typical dimensions of the polished bar-shaped specimen were 30 mm long, 4 mm wide and 4 mm thick. The flexure tests were done in a universal Instron testing machine at a crosshead speed of 0.5 mm per min.

The dielectric constants were measured on sintered disks of 6 mm dia. × 6 mm height at 1 MHz (HP 4194A Impedance/Gain-Phase Analyser and an HP 16034E electrode fixture, Hewlett-Packard).

3. Results and discussion

Fig. 3 shows a micrograph of coated hollow spheres after drying. Under optimal coating conditions there were no uncoated or partially coated spheres, and the amount of free alumina precursor grains (indicated in Fig. 3 by an arrow) was negligible. All spheres were coated with a uniform layer of small, cube-shaped alumina precursor grains with edge lengths of 1–1.5 μm. The coating thickness was determined by crushing some spheres and examining the fragments

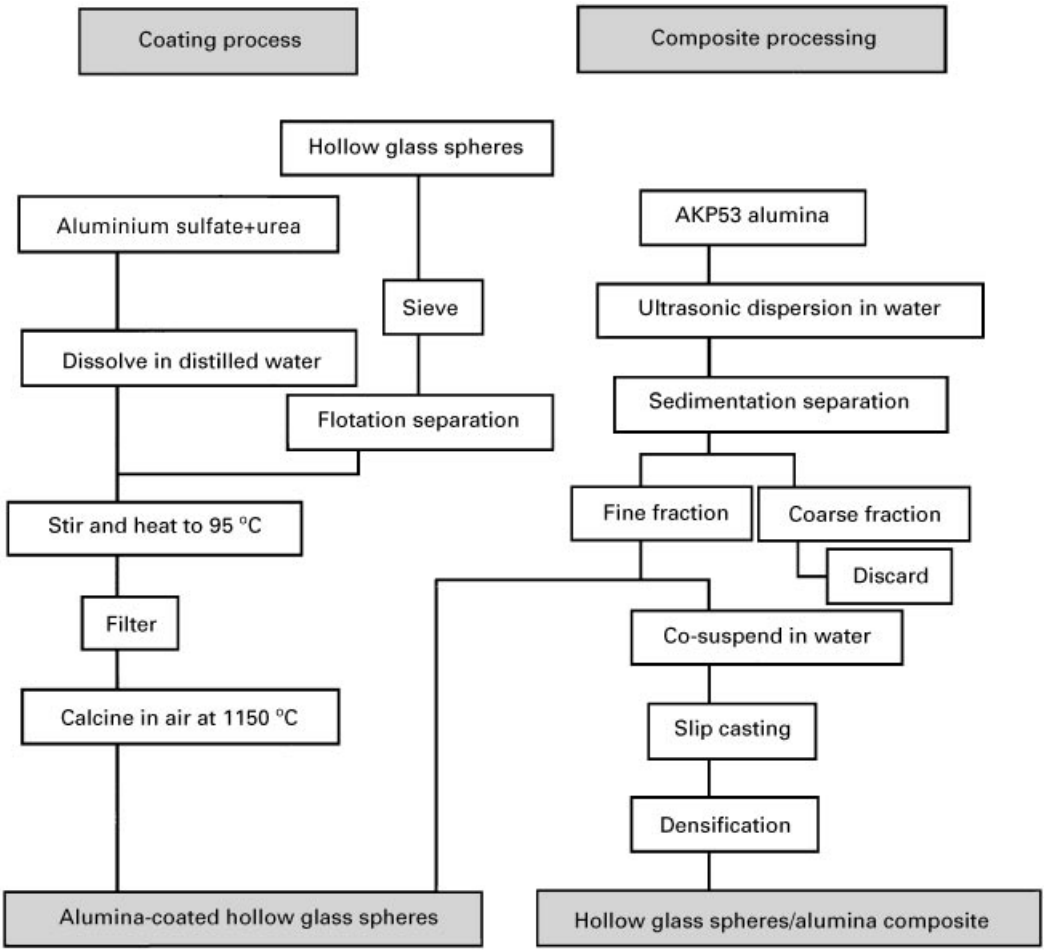

Figure 2 Flowchart of surface coating process via controlled heterogeneous nucleation in aqueous solution and of composite preparation with alumina as the continuous phase and the coated hollow spheres as the dispersed phase.

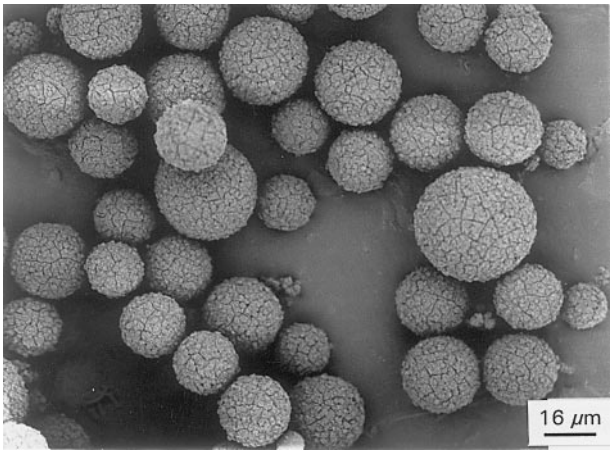

Figure 3 SEM micrograph of coated glass hollow spheres after drying. Some free alumina precursor is indicated by the arrow. Under optimum coating conditions only a negligible amount of free precursor is formed.

by SEM, yielding an average value between 1–1.5 μm. Large cracks were found in the coating layer. These cracks were most likely caused by the volume shrinkage accompanying water loss during drying. After drying, the coating layer was found to adhere well, and the coated spheres behaved like a free-flowing powder that could be handled subsequently without causing any coating detachment.

In similar coating processes used by Kapolnek and also Kapolnek and De Jonghe [4, 7] and by Mitchell *et al.* [11] the precursor was shown to consist of a mixture of several aluminium sulfate hydrate compounds, which included $Al_6O_9SO_3 \cdot xH_2O$ and $3Al_2O_3 \cdot 4SO_3 \cdot 8H_2O$. In the current experiments the aluminium precursor layer was also crystalline, as indicated by sharp X-ray diffraction peaks. However, the spectra did not have a full match to any of the patterns in the available literature. Complex crystal structures of hydrated alumina sulfates with varying water content might cause such ill-defined diffraction peaks. Since the alumina precursor was only an intermediate phase, the chemical compositions of the sulfates was not analysed further.

3.1. Optimization of coating parameters

The heterogeneous precipitation process involves close control of many parameters. Among these, the following factors were found to have the most significant effect: concentration of nucleation sites, stirring speed, and temperature. A series of experiments led to the optimization of the process conditions; in these, one of the parameters was varied for each test until a satisfactory coating was obtained.

In optimizing the coating process, it was found that varying the available surface area for nucleation, i.e., the concentration of glass spheres, was more effective

than adjusting the reactant concentrations (alumina sulfate hydrate and urea). Too high a glass sphere concentration resulted in many uncoated or partially coated spheres, while too low a concentration led to bulk precipitation of the alumina precursor and this was very difficult to remove from the suspension. Thus, control of the concentration of glass spheres was critical to achieving a good coating. The optimum range of glass spheres was relatively narrow, with the coating thickness increasing as the bulk precipitation limit was approached.

At high propeller stirring speed, hydroxyl ions released from the urea could be evenly distributed in the solution, which resulted in uniform nucleation; otherwise, local variations of pH values caused non-uniform heterogeneous precipitation which created a wide size distribution of precursor grains. Also, at locations with a high concentration of hydroxyl ions, a supersaturation of reactants (alumina sulfate) might cause homogeneous precipitation. Vigorous stirring must be maintained throughout the entire coating period to ensure good dispersion of glass spheres in the aqueous solution. The requirements of a uniform generation of hydroxyls and a good dispersion of spheres in the suspension make the stirring speed an additional important factor in the coating experiment.

The decomposition rate of urea depended mainly on the solution temperature. Too low a temperature did not release enough hydroxyl ions to initiate the precipitation reaction. On the other hand, if the coating temperature was too high, then the increased hydroxyl release rate quickly raised the pH value of the solution, again causing excessive bulk precipitation. Control of the solution temperature to within $\pm 1\,^{\circ}C$ was, therefore, one of the most critical parameters for achieving optimal and reproducible coating results.

About 18 wt % of the concentration of the original aluminium ions were precipitated from the solution to form the alumina precursor coating. This was because only those aluminium ions which exceeded the solubility limit could be depleted from the solution to form the coating. The rest of the material remained in solution and could not be precipitated out.

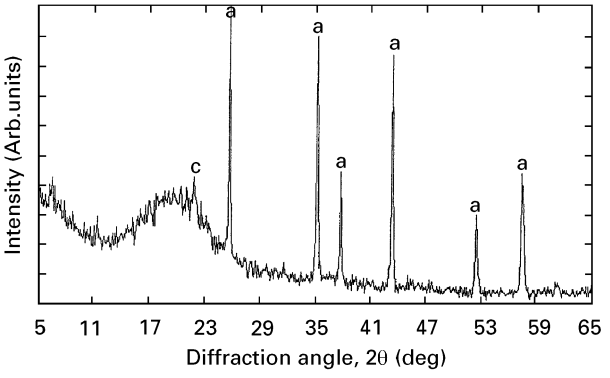

Figure 4 X-ray diffraction patterns of coated spheres after calcination at 1150 °C in air for 2 h. a: α-alumina, c: α-cristobalite.

3.2. Calcination

Calcination of the alumina precursor coating prior to sintering was necessary so that the gaseous products (mainly SO_2 and H_2O) could be removed before they were trapped inside the densified alumina matrix. XRD analysis was used to characterize the phase evolution during the firing. It was found that the alumina precursor first converted to γ-alumina at temperatures between 700–900 °C. The γ-alumina subsequently transformed completely to α-alumina at about 1150 °C, as previously reported [13–18]. Below 1150 °C, conversation to α-alumina remained incomplete. Complete conversion to α-alumina was essential for the densification of the alumina matrix, as could be expected from several other studies which have shown that densification is often impeded if starting powders transform during heating [19–22].

Fig. 4 shows an XRD pattern of coated spheres after calcination at 1150 °C for 2 h. All of the alumina precursor had been converted into α-alumina. While the majority of the glass spheres were still amorphous, as indicated by large XRD intensities below 20°, a small amount of α-cristobalite peaks were also detected.

The conversion of the alumina precursor was found to occur without any obvious change in over-all coating morphology. Fig. 5 is a comparison of the coating structure before and after calcination, clearly showing that the α-alumina grains retained the original over-all precursor shapes. However, a large weight loss ($\approx$40 wt %) accompanied the decomposition reaction due to dehydration and desulfurization, implying that the α-alumina coating layer was quite porous.

Fig. 6a shows a micrograph of coated spheres after calcination. The alumina coating layer had partially mixed with the glass. This is because the calcination temperature was higher than the softening point of the glass (1150 °C versus 900 °C), so that the glass flowed under the effect of capillary forces induced by the fine porosity in the α-alumina layer. The walls of the coated spheres after calcination could, therefore, be considered as a mixture of α-alumina grains and silica glass. This mixing phenomenon firmly bound the coating layer to the glass wall, which greatly facilitated subsequent processing.

The glass spheres remained intact and spherical, with less than 1% damage. The wall thickness of the broken spheres was always less than 0.5 μm, see Fig. 6b. Judging from their appearance, the burst-type fracture could result from an elevated internal gas pressure during calcination, exceeding the mechanical strength of the thinnest glass walls.

Both EDS and wet chemical analyses were performed on calcined samples for composition determination. They all showed similar results. The weight ratio of $Al_2O_3 : SiO_2$ was found to be 50.6 : 49.4. Evidence of the potential presence of trace amounts of sulfur was sought by RBS, but as shown in Fig. 7, no sulfur could be found by this method above the 100 ppm detection threshold.

True particle density was determined to be 1.3 $g\,cm^{-3}$ by helium gas pycnometry. The theoretical density of the solid phase was calculated to be

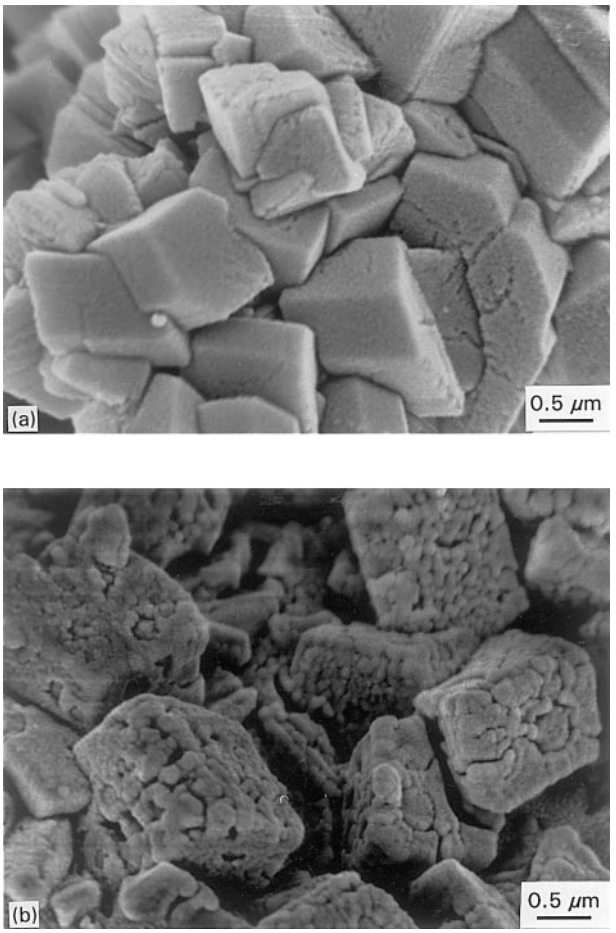

Figure 5 SEM micrographs of coated grains (a) before calcination and (b) after calcination at 1150 °C for 2 h in air. Note that α-alumina grains retained the original precursor over-all shapes after calcination.

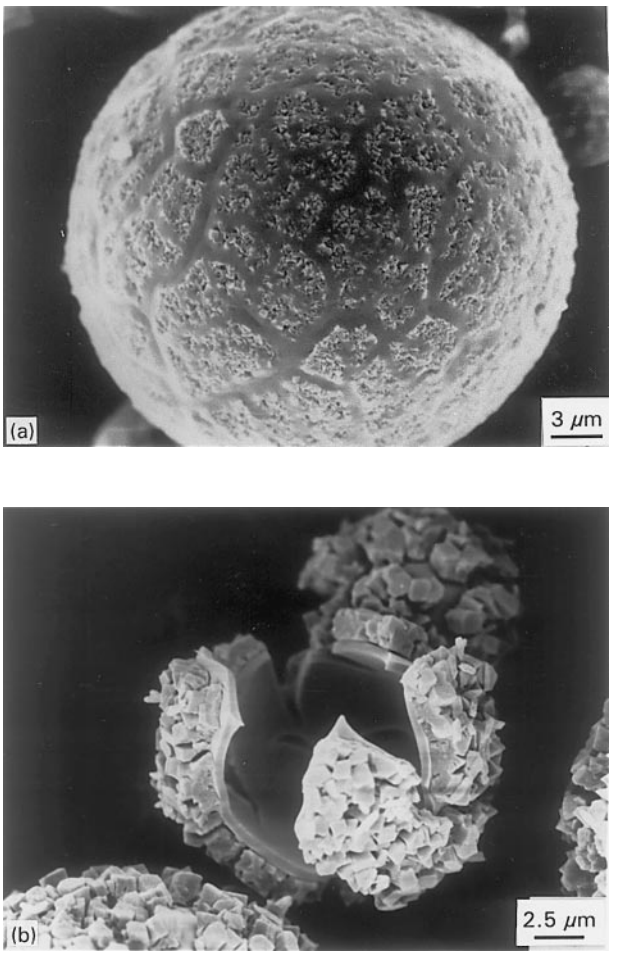

Figure 6 SEM micrographs of (a) an intact sphere after calcination and (b) a broken sphere (total amount $<1\%$). Note the lack of viscous flow of glass in (b), indicating a burst-type failure.

2.87 g cm^{-3} from the weight fractions of the alumina and the silica in the spheres. From these data the average porosity of the coated spheres after calcination was calculated to be 0.55. Compared with the porosity of uncoated hollow spheres (0.74), the coating process and calcination reduced the volume fraction of porosity significantly.

3.3. Microstructure control

The nature of porosity may be categorized into two types: inclusion pores and matrix pores. Inclusion pores are defined to be exclusively caused by intact hollow spheres. They were added to the system in a controlled manner, e.g., to reduce its dielectric constant and, therefore, a high volume fraction of inclusion pores was desired. Any pores in the matrix, including small inter- and intragranular pores as well as large pores originating from particle agglomeration and packing imperfections, were classified as matrix pores. Matrix voids cannot be controlled easily and may deteriorate the system's mechanical and hermetic properties. Although their presence would contribute to the reduction of the dielectric constant, such matrix voids were considered undesirable. When examining a polished surface under the microscope, inclusion pores are spherical, easily differentiated from the irregularly shaped matrix voids. Six groups of samples

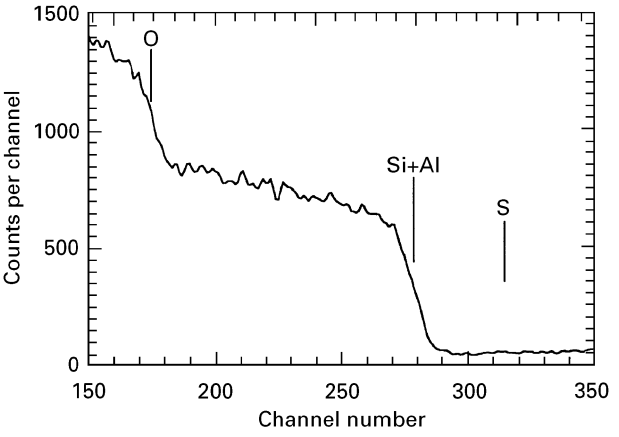

Figure 7 RBS results from coated spheres after calcination. No sulfur can be detected by this technique, meaning that its concentration is less than 100 ppm.

with an expected final porosity of about 0.10, 0.15, 0.20, 0.23, 0.33 and 0.36 were analysed. The last two groups were chosen because they corresponded to samples containing 60 vol % and 66 vol % of coated spheres, respectively, which is close to the maximum random packing density of monosized spheres (about 64 vol %).

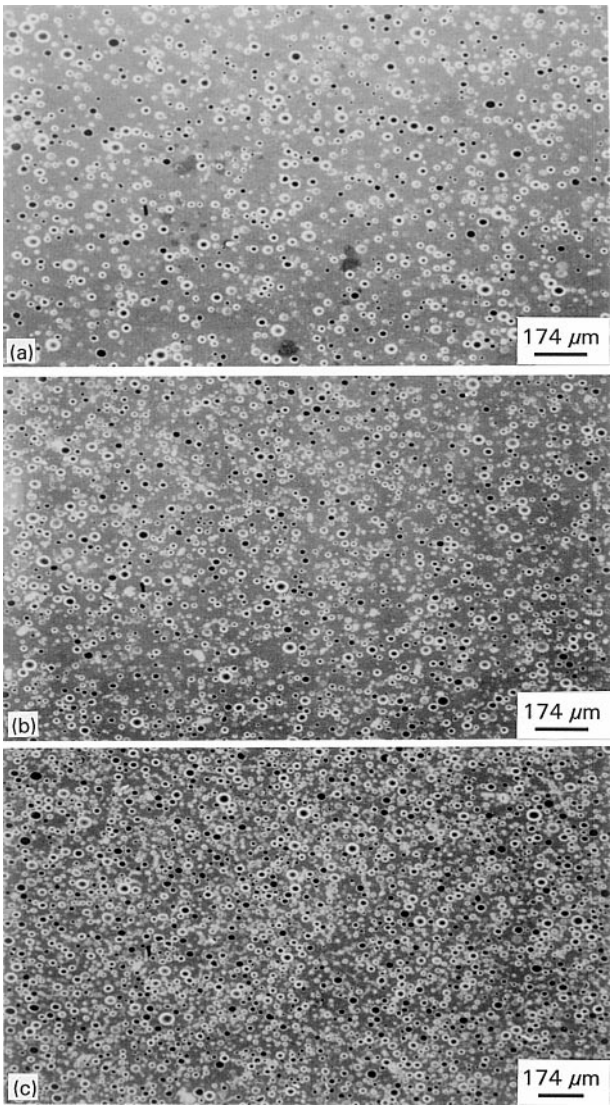

Figure 8 SEM micrographs of polished samples after sintering in air at 1400 °C (no soaking) with various porosities: (a) 9.8%, (b) 22.4% and (c) 33.9%.

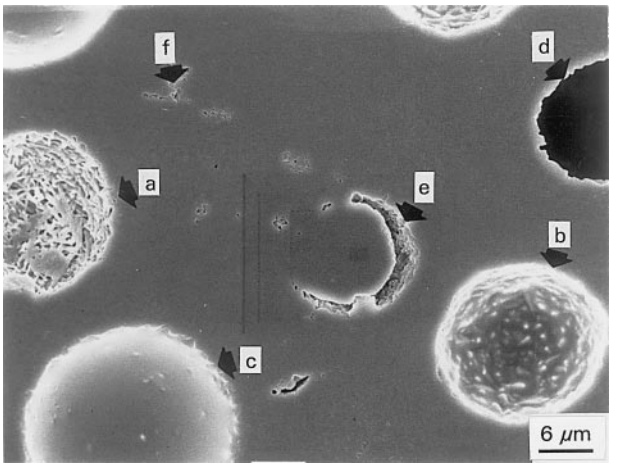

Figure 9 High magnification SEM micrograph of polished sample after sintering at 1400 °C (no soaking) in air. (a), (b), (c) and (d): pores with different morphologies, (e): voids caused by broken spheres during calcination, and (f) matrix voids.

Fig. 8 shows micrographs of polished samples with increasing porosity after sintering at 1400 °C (no soaking) in air. In all three samples pores were found to be uniformly distributed in the otherwise fully dense matrix. Neither phase segregation nor pore clusters could be observed. Since the cross-section was parallel to the direction of slip casting, this observation also proved that the slip casting process was an effective method for producing composite samples with a homogeneous distribution of the second phase (i.e., the coated spheres) in the matrix. Fig. 9 shows a typical high magnification micrograph of a sintered sample, with some residual matrix porosity indicated at (f) in this image. In this picture, the alumina matrix was found to be fairly dense. All pores were spherical in shape without deformation; however, different morphologies on the inside surface of pores were found. In pore (a), typical of the majority of pores, many well developed elongated crystallites were evident. In pore (b) elongated grains were less obvious than in pore (a); whereas in pore (c), no such elongated grains could be seen. The needle-like crystals in pores (a) and (b) were found to be mullite grains formed by the chemical reaction between Al_2O_3 and SiO_2. In the current system the low softening point glass behaved like a viscous liquid at elevated temperature, which enhanced the chemical intermixing rate of reactants and, therefore, would facilitate the grain growth of mullite in preferred directions. The different morphologies of pores (a), (b) and (c) were probably caused by the variation in thickness of the glass walls: spheres with thin walls had less glass to react with the α-alumina and, therefore, less glass would be left over after sintering. Fig. 10 illustrates an internal surface of a pore with significant quantities of elongated mullite grains. A small amount of unreacted glass was seen amid these grains. On the other hand, if spheres had thick walls then the amount of unreacted glass ostensibly increased. Large amount of residual glass would then cover the internal surface of the pores, making the newly formed mullite grains less obvious.

In Fig. 8 some pores can be seen to be very close, especially at a high volume fraction of spheres. Detailed examination found that such inclusion pores were always isolated from each other by a solid wall. The shortest pore-to-pore distance in the samples was found to be about 3 μm. Such a small distance implied that the coated glass spheres touched each other after green compact formation. In this case, if there were no coating layer between the glass spheres, connected porosity would form at the contacting area during sintering. The effectiveness of the coating in maintaining isolated porosity was further evidence by a comparison of the coated sphere composites with composites prepared from AKP53 alumina and glass spheres that were not coated. In the latter, frequent pore connections could be found, as shown in Fig. 11.

To obtain a final microstructure with a dense matrix, a sufficient amount of alumina has to be supplied to fill all interstitial spaces between the coated spheres. As the volume fraction of coated spheres increases, the relative amount of alumina $(1 - X)$, needed to fill this space, will decrease correspondingly. When the volume fraction of coated spheres reaches its maximum random packing density ($X_m \approx 0.64$),

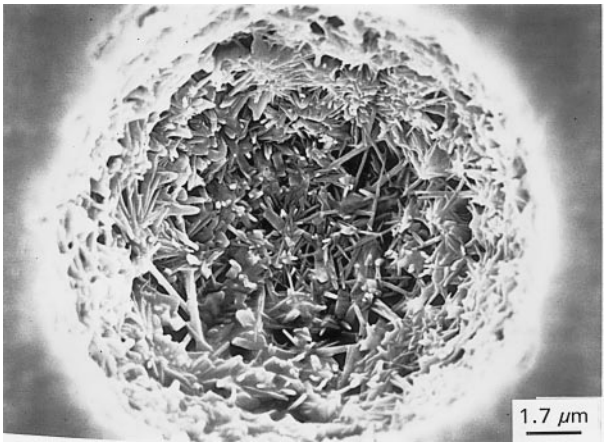

Figure 10 SEM micrograph of a pore surface after sintering at 1400 °C (no soaking) in air, showing residual glass amid elongated mullite grains.

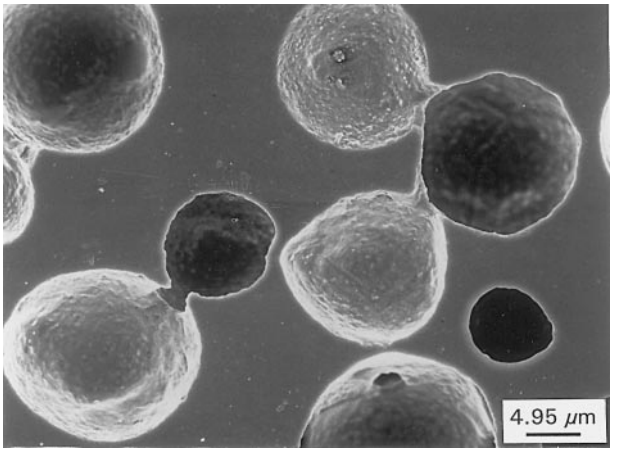

Figure 11 SEM micrograph of polished surface of sample containing 80 vol % alumina and 20 vol % as-received glass hollow spheres. Sintering was conducted at 1400 °C in air (no soaking). Interconnection between neighbouring pores are evident.

there will be just enough alumina to fill all open spaces which are left over by the densely packed spheres. With higher loading of coated spheres, i.e., when $X > X_m$, the amount of matrix alumina will not be sufficient to fill all the interstices between the coated spheres and, therefore, some voids will form in the matrix. The volume ratio of coated spheres to alumina, $X_m/(1 - X_m) \approx 1.78$, is, therefore, a theoretical loading limit when preparing green samples. Any volume ratio higher than this critical value in the original mixture will result in matrix voids, which were not desired. Fig. 12a illustrates the polished surface of a sample with sphere loading higher than the critical value (0.64 volume fraction). In this case, the sintered sample contained 0.66 volume fraction of coated spheres. A detailed examination of this sample reveals that, besides the inclusion-type spherical pores, irregularly shaped matrix voids are present, as shown in detail in Fig. 12b. Further evidence of matrix voids caused by the lack of matrix alumina is illustrated in Fig. 13, which shows a polished sample with an even higher loading of spheres (80 vol %). It is obvious that due to the limited amount of matrix α-alumina powder, continuous matrix porosity resulted. In such case,

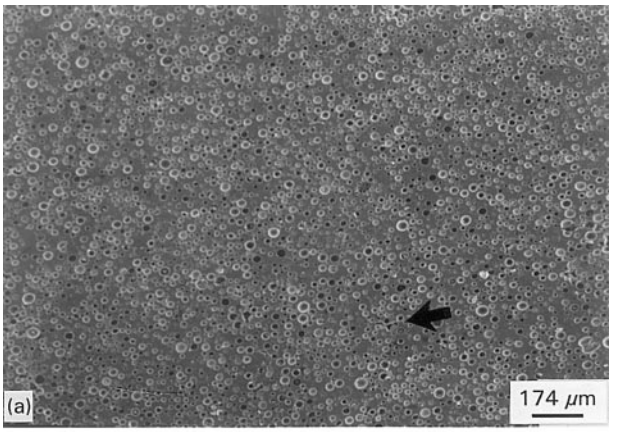

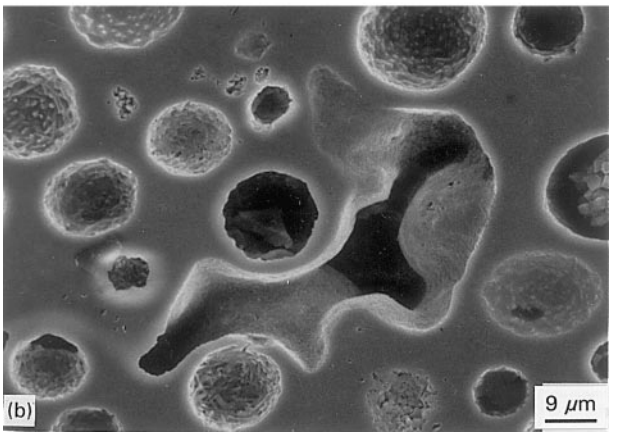

Figure 12 SEM micrographs of a polished sample (66 vol % spheres) after sintering at 1400 °C (no soaking) in air. (a) low magnification, (b) a matrix void as indicated by the arrow in (a).

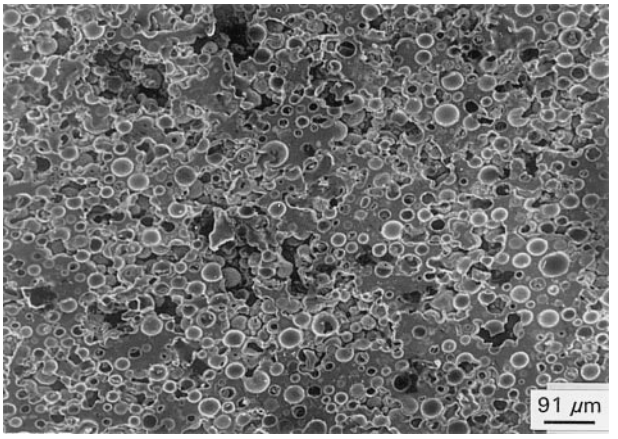

Figure 13 SEM micrograph of a polished sample after sintering containing large amounts of connected porosity due to too high loading (80 vol %) of coated glass hollow spheres.

although the volume fraction of porosity is very high, the mechanical strength and hermeticity of the sintered samples will be compromised.

3.4. Chemical composition

Quantitative analysis of the chemical composition of crystalline phases in the final products was carried out by X-ray diffraction (XRD). To determine the relative amounts of alumina and mullite in the sintered

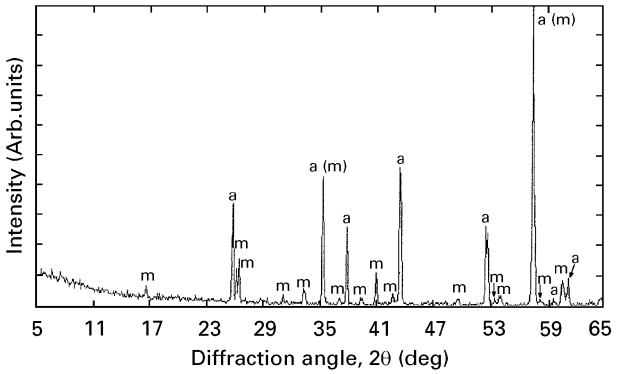

Figure 14 X-ray diffraction pattern of sample (80 wt % alumina/20 wt % coated spheres) after sintering in air at 1400 °C (no soaking). a: α-alumina, m: mullite.

sample, a calibration curve was first made by the following procedures: mixtures containing α-alumina and 5, 10, 20, … , 80 wt % mullite were mechanically mixed and analysed by X-ray diffraction. Peak ratios of the two phases were then calculated using $I_M/(I_A + I_M)$, where I_A and I_M were the areas under the α-alumina (113) peak and the mullite (121, 211) peaks, respectively. They were chosen because of their strong intensities as well as their lower overlap compared to other peaks.

The diffraction pattern of a polished sample after sintering is shown in Fig. 14. α-alumina and mullite were the only phases which could be detected under current testing conditions. However, as shown in Fig. 9, some SiO_2 was left over in some pores, but this small amount of residual glass could not be detected by the X-ray analysis. The final compositions of sintered samples should, therefore contain α-alumina, mullite, and residual glass. The relative amount of these phases depends on the initial composition of the green samples. The weight fraction of unreacted glass in the sintered sample, x, may be calculated using the relation $x = (1 - f_{\alpha t}) - (f_{\alpha t} - f_\alpha)\ 0.39$, where $f_{\alpha t}$ is the initial weight fraction of α-alumina before sintering which is set by the compositions of the green compact, and is the remaining unreacted alumina in the sintered sample determined from the XRD data, while the factor 0.39 is the ratio of the weight fraction of silica over the weight fraction of alumina in mullite ($3Al_2O_3.2SiO_2$). f_α was determined from XRD data as shown in Fig. 14.

Fig. 15 shows the final vol % of phases in sintered samples as a function of the wt % of coated spheres in the green samples. Specimens containing more than 33 wt % (60 vol %) of coated spheres were not analysed, because such samples contained matrix voids. As shown in this figure, with increasing amounts of hollow spheres, both mullite and porosity in the sintered samples increased, while alumina decreased. The final microstructure of the sintered sample can, therefore, be envisaged as a composite consisting of a dense multiphase matrix with a continuous α-alumina phase and with isolated, uniformly dispersed pores, where each pore is surrounded by a mullite/glass mixture.

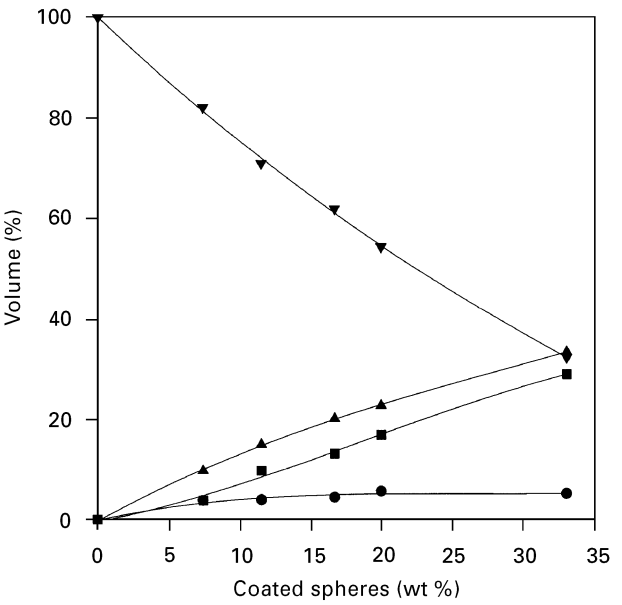

Figure 15 Volume fraction of phases in sintered samples as a function of wt % coated spheres in green samples. The symbols represent; (▼) vol % alumina, (▲) vol % porosity, (■) vol % mullite and (●) vol % glass.

3.5. Mechanical strength

Mechanical strength was evaluated in the four-point flexure mode and the results are shown in Fig. 16. Each point in this figure is the average value for 5 samples. The flexural strength of dense pure alumina is high (470 MPa). However, as expected, the flexural strength decreases rapidly with increasing porosity, p. By fitting $\sigma_\circ$, σ and p into the semi-empirical equation $\sigma = \sigma_\circ \exp(-bp)$ [23], b values were obtained which ranged from 4.0 at low porosity to 4.4 at 35 vol % porosity. It is interesting to note that the parameter b found here is significantly less porosity-dependent than is generally observed [24]. Considering the larger

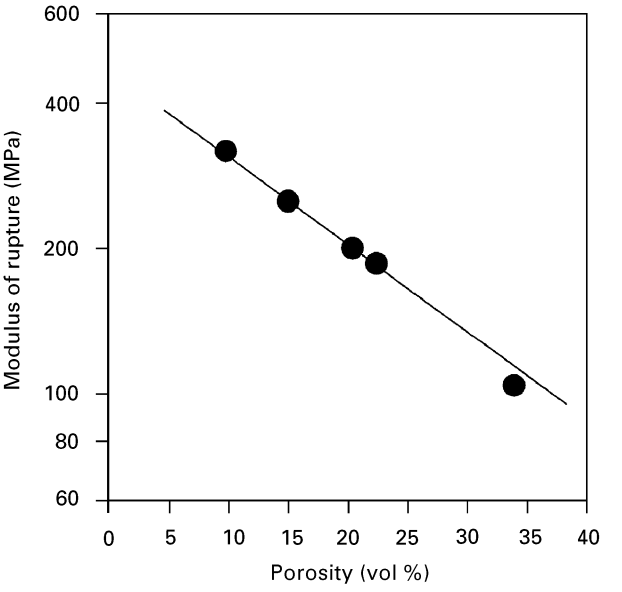

Figure 16 Flexural strength of sintered samples as a function of vol % porosity.

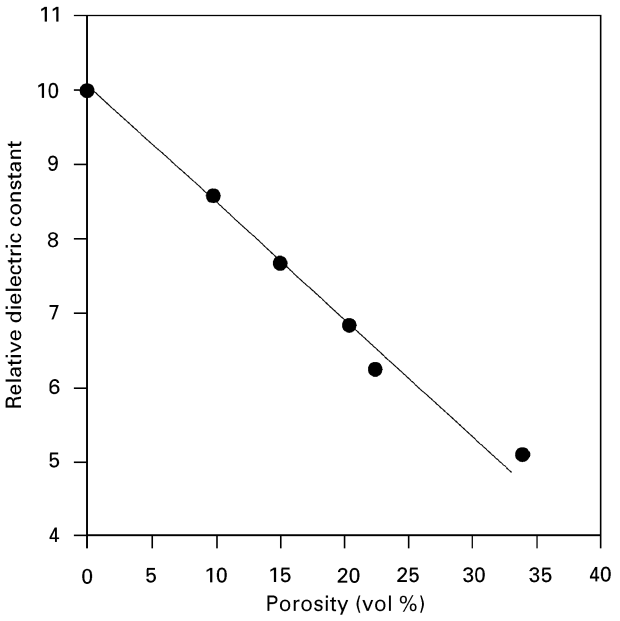

Figure 17 Measured dielectric constant of sintered samples as a function of vol % porosity.

pore sizes ($\approx$20 μm) and their large size standard deviation (about 10 μm), such relatively low b values are an indication that the current fabrication technology can be effective in preventing a rapid decline of the mechanical strength of the ceramic composites with increasing porosity. At 34 vol % porosity the flexural strength was still 105 MPa. This value could still meet current microelectronics application requirements. [29, 30].

3.6. Dielectric constant

The results of the dielectric constant measurements are shown in Fig. 17. The dielectric constant decreases almost linearly with increasing volume fraction of pores. This lack of agreement with general mixing models such as the Maxwell model is likely to be due to the changing phase composition with increasing porosity. With 33 wt % spheres (60 vol % spheres and 0.34 final porosity) a relative dielectric constant of the composites as low as 5.1 was obtained. Composites with properties as prepared here may have application in microelectronics packaging [25–30].

Conclusions

Uniform coatings of glass hollow spheres have been realized using a controlled heterogeneous precipitation method. A variety of processing conditions affect the outcome of the coating process; these include the concentration of nucleation sites, the stirring speed, and the solution temperature. By proper adjustment of these parameters, reproducible coating layers could be obtained. After calcination, converting the precursor into α-alumina, the coated spheres constitute a free-flowing powder. Alumina/coated sphere composites were prepared and their chemical composition and microstructure was evaluated. Isolated pores, well dispersed into a dense ceramic matrix, were obtained up to about 33 vol % of porosity. The mechanical properties and dielectric constant of such porous composites were determined. Dielectric constants as low as 5.1 were obtained.

Acknowledgements

Partial support for S. J. Wu from the Nisshin Steel Corporation is gratefully acknowledged. This work was supported by the Director, Office of Energy Research, Office of Basic Energy Sciences, Materials Sciences Division of the US Department of Energy, under contract No. DE-AC03-6-76SF00098.

References

1. P. E. DEBELY, E. A. BARRINGER and H. K. BOWEN, *J. Amer. Ceram. Soc.* **68** (1985) C76.
2. R. K. ILER, *ibid*, **47** (1964) 194.
3. T. GARINO, *ibid*, **75** (1992) 514.
4. D. KAPOLNEK, M.S. thesis, University of California, Berkeley, May 1989.
5. A. K. GARG and L. C. DE JONGHE, *J. Mater. Res.* **5** (1990) 136.
6. M. SACKS, N. BOZKURT and C. SCHEIFFELE, *J. Amer. Ceram. Soc.* **74** (1991) 2428.
7. D. KAPOLNEK and L. C. DE JONGHE, *J. Euro. Ceram. Soc.* **7** (1991) 345.
8. S. KRATOHVIL and E. MATIJEVIC, *Advances Ceramic Mat.* **2** (1987) 798.
9. B. FEGLEY Jr., P. WHITE and H. K. BOWEN, *J. Amer. Ceram. Soc.* **68** (1985) C60.
10. H. OKAMURA, E. BARRINGER and H. K. BOWEN, *ibid*, **68** (1986) C22.
11. T. MITCHELL Jr., L. DE JONGHE, W. MOBERLYCHAN and R. O. RITCHIE, *ibid*, **78** (1995) 97.
12. L. GORDON, M. L. SALUTSKY and H. H. WILLARD, "*Precipitation from Homogeneous Solution*" (Wiley, New York 1959). Ch. 2.
13. J. E. BLENDELL, H. K. BOWEN and R. L. COBLE, *Am. Ceram. Soc. Bull.* **63** (1984) 797.
14. B. C. CORNILSEN and J. S. REED, *ibid*, **58** (1979) 1199.
15. F. F. LANGE, *J. Am. Ceram. Soc.* **67** (1984) 83.
16. F. W. DYNYS and J. W. HALLORAN, *ibid*, **67** (1984) 596.
17. K. KENDALL, in *British Ceramic Proceedings, No. 42*: Complex Microstructure, edited by R. Stevens and D. Taylor (Institute of Ceramics, Shelton, 1989) pp. 81–90.
18. M. D. SACKS, T. Y. TSENG and S. Y. LEE, *J. Amer. Ceram. Soc.* **63** (1984) 301.
19. C. J. P. STEINER, R. M. SPRIGGS and D. P. H. HASSELMAN, *ibid*, **55** (1972) 115.
20. D. I. MATKIN, W. MUNRO and T. M. VALENTINE, *J. Mater. Sci.* **6** (1971) 974.
21. A. C. D. CHAKLADER and L. G. MCKENZIE, *J. Amer. Ceram. Soc.* **49** (1966) 477.
22. P. A. BADKAR and J. E. BAILEY, *J. Mater. Sci.* **11** (1976) 1794.
23. E. RYSKEWITCH, *J. Amer. Ceram. Soc.* **36** (1953) 65.
24. L. F. NIELSEN, *ibid*, **73** (1990) 2684.
25. J. F. MACDOWELL and G. H. BEALL, *in Ceramic Transactions, Vol. 15: Materials and Processes for Microelectronic Systems*, edited by K. M. Nair, R. Pohanka and R. Buchanan (American Ceramic Society, Westerville, OH, 1990).
26. D. W. KELLERMAN and R. PELUSO, *ISHM Proceedings.* (1990) pp. 345–51.
27. M. J. LEAP, W. HUEBNER and I. EICHER, in "Ceramic Substrates and Packaging for Electronic Application", *Advances in Ceramics*, Vol. 26 edited by M. F. Yan, K. Niwa, H. M. O'Byan Jr and W. S. Young (The American Ceramic Society, Westerville, OH, 1987) 399.

28. P. SLIVA, L. E. CROSS, T. R. GURURAJA and B. E. SCHEETZ, *Mat. Let.* **4** (1986) 475.
29. K. G. EWSUK, in *Ceramic Transaction, Vol. 15: Materials and Processes for Microelectronic Systems*, edited by K. M. Nair, R. Pohanka, and R. Buchanan (American Ceramic Society, Westerville, OH, 1990) pp. 279–95.
30. R. R. TUMMALA, *J. Amer. Ceram. Soc.* **74** (1991) 859.
31. Y. SHIMADA, Y. YAMASHITA and H. TAKAMIZAWA, *IEEE Trans. Comp. Hybrids Manuf. Technol.* **11** (1988) 163.

Received 21 August 1995
and accepted 18 March 1996